Journal of Catalysis 399 (2021) 75–85

Contents lists available at ScienceDirect

Journal of Catalysis

journal homepage: www.elsevier.com/locate/jcat

PERSPECTIVE

Developing quantitative synthesis-structure-function relations for framework aluminum arrangement effects in zeolite acid catalysis

Elizabeth E. Bickel, Claire T. Nimlos, Rajamani Gounder *

Charles D. Davidson School of Chemical Engineering, Purdue University, 480 Stadium Mall Drive, West Lafayette, IN 47907, USA

ARTICLE INFO

Article history:
Received 8 March 2021
Revised 23 April 2021
Accepted 26 April 2021
Available online 4 May 2021

Keywords:
Al arrangement
Al distribution
Brønsted acid catalysis
Synthesis-structure–function relations
Zeolites

1. Introduction

Aluminosilicate zeolites have long been recognized to behave as a catalytically diverse suite of solid Brønsted acids [1-3], in part because their framework topologies possess a wide range of micropore sizes (<2 nm in diameter) and shapes (e.g., channels, pockets, cages) [4,5], which influence reactivity via shape-selective and diffusion-related phenomena [3,6,7]. A landmark study by Haag and co-workers in the early history of zeolite acid catalysis reported a structure–function relation that suggested proton sites in zeolites were equally reactive, based on *n*-hexane cracking rates (per gram) that increased linearly with Al content (per gram) among H-MFI zeolites of widely varying composition (Si/Al = 15–10,000) [8]. The authors concluded that these data reflected catalytically-equivalent protons among the 26 unique framework O atoms in MFI [8], but also acknowledged an alternate explanation wherein the zeolite samples studied contained similar distributions of catalytically distinct protons, despite their varying composition [9].

Recent advances in zeolite synthesis [10] have provided access to zeolite materials with Al substituted in distinct framework locations [11,12] and arrangements [13,14], resulting in reports that catalytic diversity can arise from the specific locations and arrangements of Al among crystallographically distinct tetrahedral sites (T-sites) and site ensembles in zeolite lattices. Al location determines the lattice O atoms capable of hosting charge-compensating proton active sites, and in turn the microporous voids within which reactive intermediates and transition states reside, and thus the extent to which they are stabilized by confinement effects [15,16]. Furthermore, Al-Al site pair ensembles of differing relative proximity (i.e., Al-(O-Si)$_x$-O-Al; $x \geq 1$) have been reported to result in different turnover rates (e.g., alkane cracking [17,18], alkene oligomerization [19,20]) and product selectivities (e.g., methanol-to-olefins [21,22]) for acid-catalyzed reactions relevant to industrial processes, highlighting that the design of zeolites with different Al siting and arrangement is an emerging strategy in catalyst development for commercial applications. Additionally, the framework Al arrangement influences the structure and speciation of exchanged metal ions and complexes that are precursors to active sites for methane partial oxidation [23-26] and dehydroaromatization [27-29], alkane dehydrogenation [30-32], and various redox and decomposition reactions of nitrogen oxides [33-39]. Our perspective on the effects of Al location among distinct T-sites and void environments on zeolite acid catalysis can be found elsewhere [16], and this Perspective focuses solely on the effects of different Al-Al site pair ensembles on acid catalysis.

The increasing recognition that turnover rates for certain acid-catalyzed reactions depend on framework Al arrangements in zeolites motivates a critical reassessment of the underlying components of the structure–function relation reported by Haag and co-workers

* Corresponding author.
E-mail address: rgounder@purdue.edu (R. Gounder).

https://doi.org/10.1016/j.jcat.2021.04.027
0021-9517/

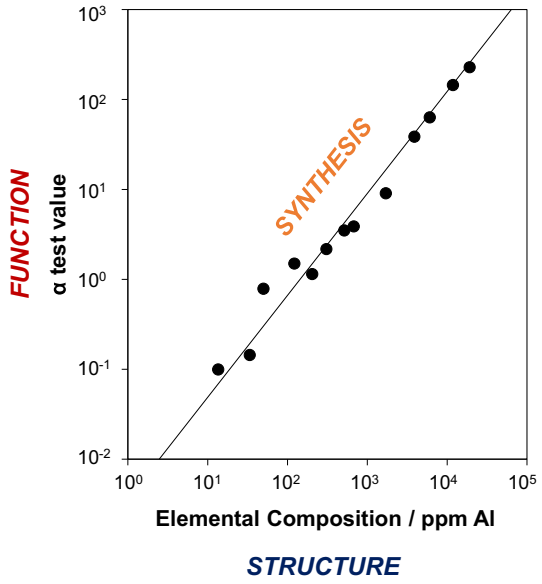

Fig. 1. A structure–function relation for the equivalent reactivity (“alpha” test value, α, calculated as the rate of *n*-hexane cracking on a zeolite sample relative to a 10 wt% Al_2O_3 amorphous silica-alumina reference) of acid sites in MFI zeolites of varying composition; data reported originally by Haag et al. [8]. Contemporary data describing the effects of Al location and arrangement on turnover rates of acid-catalyzed reactions motivate revisiting the underpinnings of the three components of a synthesis-structure–function relation.

(Fig. 1) [8]. This relation implies, at first glance, that acid site proximity does not influence catalysis given that adjacent Al sites become closer in proximity, on average, with increasing framework Al content [40]. The development of rigorous structure–function relations that describe Al arrangement effects in zeolite acid catalysis requires underlying mechanistic connections, and thus is predicated on methods that can quantify putative active site ensembles and quantify catalytic function using turnover rates for distinct site ensembles. Additionally an often overlooked but critical component underlying any structure–function relation concerns the specific methods used to synthesize the materials under interrogation, and therefore the consequences of such synthetic methods on the site ensembles that are formed. Herein, we identify and discuss pertinent research questions underlying the three components of a synthesis-structure–function relation:

(i) Structure: What methods quantitatively characterize distinct proton-proton active site ensembles or the distinct Al-Al site pair ensembles that serve as their structural surrogates?
(ii) Function: How can differences in catalytic reactivity at distinct active site ensembles be identified in experimental measurements and interpreted mechanistically?
(iii) Synthesis: What synthetic approaches enable preparation of different Al-Al site pair ensembles in low- and high-symmetry zeolite frameworks, as required to obtain materials that can be interrogated to recognize differences in site arrangement-dependent reactivity?

In this Perspective, we discuss current challenges that prevent more precise definitions of the three components comprising quantitative synthesis-structure–function relations for Al arrangement effects in zeolite acid catalysis. Our viewpoint is that the catalytic consequences of framework Al arrangement are discernable and rigorously interpretable via quantitative measurements in the form of turnover rates that are uncorrupted by bed-scale and intracrystalline concentration and temperature gradients [41]; however, such interpretations require methods to accurately quantify distinct proton-proton and Al-Al site pair ensembles in zeolites. We describe recent advances in quantitative approaches to experimentally characterize the structure and reactivity of distinct Al-Al site pair ensembles in zeolites, which can be validated by theoretical models. We focus on chabazite (CHA) zeolites because they can be synthesized over a wide composition range (Si/Al = 1–∞), which engenders synthetic versatility, and because they contain only one crystallographically-unique T-site, which simplifies the interpretation of experimental characterization data and enables more faithful connections to theoretical models. Exhaustive approaches to developing Al arrangement models become less tractable for lower-symmetry zeolite frameworks, such as MFI. We conclude with our perspective on best practices to define and quantify Al arrangements in zeolites and the pertinent challenges and opportunities for future research.

2. High-symmetry zeolite frameworks simplify Al siting models and investigations of acid site proximity effects in catalysis

The stability of reactive intermediates and transition states that mediate Brønsted acid-catalyzed reactions in zeolites depends on acid strength and confinement. A probe-independent definition of acid strength, deprotonation energy (DPE), is the energy required to separate a proton from its conjugate base (i.e., the deprotonated lattice $[AlO_{4/2}]^-$ center) to non-interacting distances; DPE values depend only weakly on the structure and geometry of crystallographically unique T-sites for the case of a single Al center [42]. By contrast, confinement effects reflect the solvation of transition states and reactive intermediates by van der Waals interactions with the zeolite lattice, which depend strongly on the structure and geometry of the microporous voids within which H^+ sites reside; thus, turnover rates of Brønsted-acid catalyzed reactions (e.g., dimethyl ether carbonylation [43], alkane cracking and dehydrogenation [44,45], alkene hydrogenation [46], alkylation [47], and oligomerization [48], alkanol dehydration [49,50], and acetone condensation [51]) differ among acid

sites confined within zeolitic voids of different size and shape [16,52,53]. Consequently, high-symmetry zeolite frameworks serve as model materials that simplify the interrogation of the catalytic behavior of distinct Al-Al site pair ensembles, because they restrict the number of unique crystallographic locations at which Al can reside.

2.1. Experimental and theoretical assessments of Al arrangement models in CHA frameworks

CHA frameworks contain a single crystallographically unique T-site and are composed of double 6-MR composite building units assembled to form large cavities (i.e., cages that are ~ 8 Å in diameter and ~ 12 Å in height) with access limited by 8-membered ring (8-MR) apertures (i.e., windows that are ~ 4 Å in diameter) [54]. Each T-atom is bonded to 4 crystallographically-distinct O atoms, each of which is associated with three distinct (alumino)siloxane rings composed of 4, 6, or 8 T-atoms. The Al content of each X-MR can vary between 0 and X/2 while adhering to Löwenstein's rule [55], which disallows Al substitution in nearest neighbor (NN) lattice positions. Statistical simulations can enumerate the populations of Al in the different ring structures of CHA for a given Si/Al ratio upon enforcing certain constraints or biases (e.g., a random substitution that obeys Löwenstein's rule) [56]. Statistical simulations of Al arrangements in CHA showed that the fraction of 6-MRs containing multiple Al substituents (2 or 3) increases systematically with decreasing Si/Al ratio. Although 3 Al can be substituted in a 6-MR in an arrangement that does not violate Löwenstein's rule, such arrangements represent a minor fraction (<0.01) of the Al-Al site ensembles present in compositions of CHA commonly used as acid catalysts (Si/Al > 10) [56]. From these statistical models, we conclude that the dominant Al-Al site pair ensembles in CHA are comprised of 6-MRs that contain 2 Al atoms separated by 1 or 2 Si atoms (NNN, NNNN) [56]. Although this specific model assumes that the distribution of framework Al is random (subject to Löwenstein's rule), analogous statistical models for predicting framework Al arrangements can be readily developed by incorporating Al siting biases that reflect the influence of different synthesis conditions. Furthermore, ^{29}Si MAS NMR spectra of CHA (Si/Al = 15) with 6-MR Al-Al site pairs show resonances associated with Q^4(0Al) sites (Si-(O-Si)$_4$, −111 ppm) and Q^4(1Al) sites (Si-(O-Si)$_3$-(O-Al), −105 ppm), but insignificant quantities of Q^4(2Al) sites, suggesting that the 6-MR Al-Al pairs predominantly consist of third-nearest neighbor (3NN) Al atoms [57].

The ability of certain divalent cations to preferentially exchange distinct subsets of Al-Al site pairs in a given zeolite provides an opportunity to develop experimental titration procedures to quantify particular site ensembles. Density functional theory (DFT)-calculated energies of Co^{2+} and Cu^{2+} cations sited at different Al-Al pairs in CHA indicate an energetic preference ($\geq$20 kJ mol^{-1}) for site pairs in 6-MRs over those in 4- and 8-MRs [58]. Co^{2+} is a practical choice for experimental titration experiments because aqueous solutions can be prepared of sufficiently low pH (3–6) that predominantly contain divalent metal-aquo complexes in solution (i.e., negligible concentrations of metal hydroxide or oxide complexes) [59] while minimizing zeolite dealumination. The specific conditions that enable selective exchange of Co^{2+} at all Al-Al site pairs on a given zeolite can be determined from experimentation, such as through the measurement of an ion-exchange isotherm, supplemented with quantitative characterization of the Co structures formed on the solid. An example of quantitative characterization data is a cation site balance, in which residual H^+ sites on partially Co-exchanged zeolites are titrated by NH_3 and quantified via temperature programmed desorption (TPD), yielding a 2:1 H^+:Co^{2+} exchange stoichiometry when only isolated Co^{2+} ions are present [57].

The practicality of using Co^{2+} titrants has led to their widespread adoption as experimental probes of Al-Al site pairs in zeolites, but caution must be exercised to avoid over-interpretation of characterization data in developing Co^{2+} siting models. The speciation of Co as isolated ions and clustered oxides is readily probed by diffuse reflectance UV–visible spectroscopy (DRUV–Vis); however, d-d transition bands in UV–Vis spectra of Co-form zeolites cannot be deconvoluted to identify the locations of Co^{2+} ions located at distinct X-MR binding sites. Even at the ambient temperatures routinely used to measure UV–Vis spectra, a single cation at a given X-MR binding site will undergo changes in coordination environment due to thermally-induced vibrations that alter ring conformations and cause restructuring during the timescale of spectral acquisition, as we have demonstrated in the case of Cu^{2+} exchanged in CHA [60]. Moreover, d-d transition features that have been ascribed to Co^{2+} located within distinct X-MR structures in zeolites are also observed for Co^{2+} exchanged onto amorphous supports (e.g., SiO_2/Al_2O_3, Al_2O_3, ZnO) [61-63], which include ring structures that are distinct from those found in zeolitic frameworks, suggesting these features do not only arise from Co^{2+} bound at distinct zeolitic (alumino)siloxane ring structures [64]. Additionally, studies suggest Co^{2+} cations may exchange at defect sites present within amorphous domains and at Brønsted-Lewis acid site pairs under the aqueous-phase ion-exchange conditions that also titrate Brønsted acid site pairs [65,66]. These observations emphasize that interpretations of Co^{2+} titration data solely in terms of framework Al arrangement require additional characterization data (e.g., a cation site balance on framework Al exchange sites).

A proton may reside at one of the four distinct O atoms associated with an Al center and be oriented into a 4-, 6-, or 8-MR, each of which has a distinct O-H vibrational stretching frequency and molar absorptivity. The arrangement of protons compensating 6-MR paired or isolated Al sites in CHA can be assessed by examining OH stretching features in IR spectra, which reflect the composite vibrations of distinct proton site types. For an isolated Al center, a proton bound to each of the four O atoms yields isoenergetic structures (within 10 kJ mol^{-1}); thus, the Boltzmann-averaged population of protons at the four distinct O atoms and composite OH IR spectra are essentially temperature-independent [18]. For a 6-MR Al-Al site pair, configurations in which H^+ sites are harbored within different X-MRs are preferred because they minimize energetic penalties associated with H^+-H^+ interactions. Integrated peak areas for OH IR bands (3575 and 3600 cm^{-1}) increase systematically with increasing fractions of 6-MR Al-Al site pairs at fixed temperature (Fig. 2a) because of energetically favorable interactions across the 6-MR ring between a H^+ and the oxygen associated with a nearby Al in a 6-MR pair, which result in higher molar absorptivities. Higher energy H^+-H^+ site configurations, which yield lower molar absorptivities, become more populated with increasing temperature, resulting in a systematic decrease in the intensity and differences in shape of composite OH IR bands with increasing temperature for CHA samples that contain 6-MR Al-Al site pairs [18]. Importantly, this study demonstrates that comparison of OH IR spectral data on H-CHA at fixed temperature can enable direct characterization of certain arrangements of H^+-H^+ site pairs, and thus serves to substantiate estimates of 6-MR Al-Al site pairs determined by Co^{2+} titration.

2.2. Synthesis of CHA zeolites with varied framework Al arrangements

The framework Al arrangement in zeolites depends on the conditions of crystallization and on the structure and charge of the structure-directing agents (SDAs) used. SDA cations are organic or inorganic molecules that become occluded within different rings and voids of the

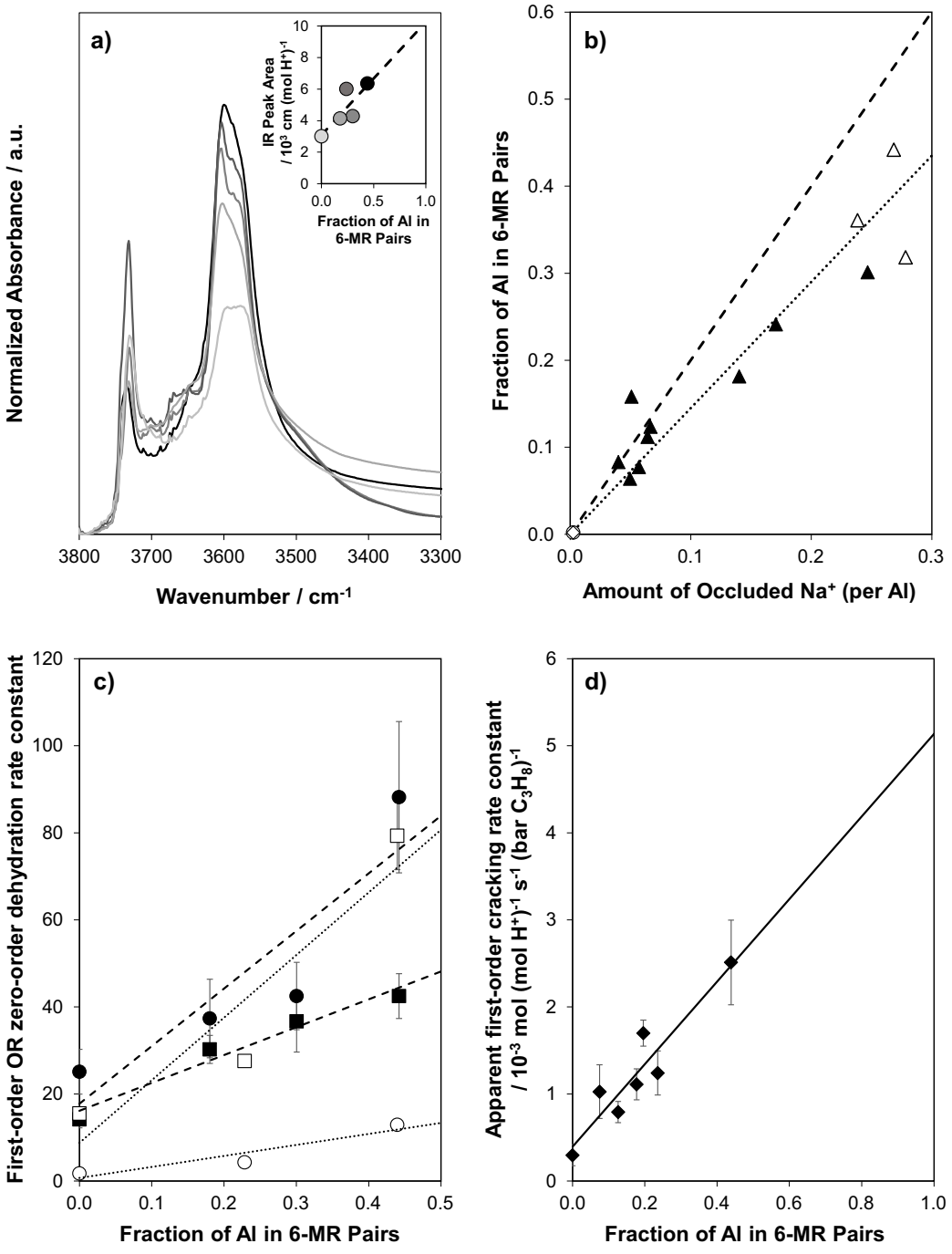

Fig. 2. (a) Normalized IR spectra (415 K) of H-CHA zeolites of similar Al content (Si/Al = 14.8–16.2) with varying fraction of Al in 6-MR site pairs (0.00–0.44, light to dark); inset shows integrated Brønsted OH stretching area with increasing fraction of Al in 6-MR site pairs, and contains a dashed line to guide the eye. (b) Fraction of Al in 6-MR pairs in H-CHA samples of similar composition (Si/Al = 14–17) plotted against the amount of Na^+ co-occluded with $TMAda^+$ on CHA synthesized with $Al(OH)_3$ and $Na^+/TMAda^+$ = 0–2 in OH^- media (▲) and $Na^+/TMAda^+$ = 0 in F^- media (◯) or with $Al(O\text{-}i\text{-}Pr)_3$ with $Na^+/TMAda^+$ = 1 (△) and $Na^+/TMAda^+$ = 0 (◇); dashed line denotes parity line (slope: 2) expected if each occluded Na^+ led to formation of a 6-MR site pair, while the dotted line represents best-fit linear regression of the data (slope: 1.45). (c) First-order methanol (●, 10^{-3} mol DME (kPa mol H^+ s)$^{-1}$), first-order ethanol (◯, 10^{-4} mol DEE (kPa mol H^+ s)$^{-1}$), zero-order methanol (■, 10^{-3} mol DME (mol H^+ s)$^{-1}$), and zero-order ethanol (□, 10^{-4} mol DEE (mol H^+ s)$^{-1}$) dehydration rate constants (415 K) plotted against the fraction of in 6-MR pairs; lines represent best-fit linear regression of the methanol (dashed) and ethanol (dotted) dehydration rate constants, respectively. Fraction of Al in 6-MR site pairs quantified by Co^{2+} titration. (d) Apparent first-order propane cracking rate constants (748 K, per H^+) on H-CHA zeolites plotted against the fraction of Al in 6-MR pairs; solid line represents best-fit linear regression of the data. Figure reproduced from [18,58,67]

crystallizing framework while compensating anionic framework charges. Crystallization of CHA from amorphous Si and Al precursors in the presence of only N,N,N-trimethyl-1-adamantylammonium cations ($TMAda^+$) leads to the predominant formation of 6-MR isolated Al sites, over a wide range of Al content (Si/Al ≥ 15) [57], because spatial constraints limit occlusion to one $TMAda^+$ (and thus one framework Al) per CHA cage (Si/Al = 11). Crystallization of CHA in the presence of both $TMAda^+$ and Na^+ cations allows their co-occlusion in a single CHA cage unit, providing a route to increase the number of framework Al to > 1 per cage (Si/Al < 11) [22,57]. Moreover, for CHA samples of essentially constant Si/Al ratio (14–17), 6-MR paired Al sites are formed in amounts that increase linearly with the amount

of Na^+ cations that are co-occluded with $TMAda^+$ (Fig. 2b). DFT energies have been computed for different arrangements of two Al in a CHA unit cell (96 T-atoms) charge-compensated by $TMAda^+$ and Na^+ occluded in various ring structures or cages, and indicate that Na^+ and $TMAda^+$ typically show an energetic preference (10–30 kJ mol^{-1}) to co-occlude in configurations where Na^+ is located in the 6-MR adjacent to the CHA cage containing $TMAda^+$ rather than in separate cages [58]. The lowest energy arrangements of two Al charge-compensated by co-occluded Na^+ and $TMAda^+$ reflect 3NN arrangements in the same 6-MR or 8-MR of CHA. These findings rationalize why co-incorporation of $TMAda^+$ and Na^+ during CHA crystallization results in an increase in the fraction of 6-MR Al pairs, consistent with experimental observations [58].

Crystallization of CHA can also occur in the presence of K^+. Unlike Na^+, K^+ competes with $TMAda^+$ for occlusion within CHA void spaces, resulting in a systematic decrease in occluded $TMAda^+$ content with increasing amounts of occluded K^+ on CHA materials [58]. Competitive occlusion of $TMAda^+$ and K^+ in CHA was further substantiated by DFT-estimated energies (96 T-atom unit cell) that revealed an energetic preference for K^+ to reside in the 8-MR windows of CHA rather than to co-occlude with $TMAda^+$ within the same CHA cage like Na^+ prefers, possibly a consequence of the larger ionic radius of K^+ relative to Na^+ [58]. CHA synthesized with K^+ and $TMAda^+$ contained predominantly 6-MR isolated Al (≥90%), consistent with DFT-computed energies indicating that 8-MR 3NN Al pairs are the most energetically favorable arrangement of two Al charge-compensated by co-occluded K^+ and $TMAda^+$ [58]. These results suggest using K^+ as an inorganic SDA results in Al arrangements (e.g., 8-MR Al-Al site pairs) distinct from those formed when $TMAda^+$ alone, or Na^+ and $TMAda^+$ together, are used as SDAs. In other studies, the fraction of $Q^4(2Al)$ sites in CHA crystallized with $TMAda^+$ and different alkali cations (Li^+, Na^+, K^+, Cs^+; Si/Al = 8–10) decreased with increasing ionic radius of the alkali cation [68]. Crystallization of CHA (Si/Al = 2) in the presence of Sr^{2+} and K^+ as co-SDAs resulted in higher fractions of $Q^4(2Al)$ (0.51–0.58) than when K^+ alone was used as an SDA (0.46–0.47) [69]. Generally, these findings highlight the importance of understanding how SDA-framework interactions govern their occlusion within specific rings and void spaces of zeolite frameworks and thereby influence the energetics of distinct arrangements of Al-Al site pairs.

CHA zeolites can also be obtained by other synthetic and post-synthetic routes that also influence Al arrangement. In the presence of $TMAda^+$, CHA synthesized by the interconversion of FAU zeolites (i.e., a non-amorphous source of Si and Al) contained higher Al contents and significantly higher fractions of 6-MR paired Al sites (0.1–0.6) than CHA synthesized from amorphous Al precursors (0.0), and the fraction of 6-MR paired Al sites formed was found to depend on certain synthesis parameters (e.g., time, temperature, gel composition) [25]. Interconversion of MFI to CHA resulted in predominantly 6-MR isolated Al, while interconversion of FAU to CHA with similar Al contents did not; this observation was attributed to possible differences in the dissolution kinetics of MFI compared to FAU during synthesis [25]. These studies demonstrate that interzeolite conversion routes provide access to distinct Al arrangements [25,70–73] other than those known to be accessible via direct hydrothermal crystallization.

2.3. Influence of Al arrangement in CHA zeolites on catalytic function

The catalytic function of CHA zeolites of fixed composition is influenced by Al arrangement for reactions wherein distinct Al-Al pair site ensembles influence the stability of reaction intermediates and transition states by introducing interactions between neighboring adsorbates or H^+ sites. For example, OH groups associated with arrangements of two Al in the 6-MR of CHA behave as stronger acids than those associated with isolated Al (larger DPE values by > 10 kJ mol^{-1}) because the deprotonated $[AlO_{4/2}]^-$ conjugate base is stabilized by hydrogen bonding with the proximal H^+ site across the 6-MR [74]. This specific mechanism for stabilizing the conjugate base requires that spectating proton sites remain uncovered, and thus is irrelevant for catalysis under conditions wherein proton sites are occupied by physisorbed or chemisorbed intermediates, as occurs during low-temperature alkanol dehydration catalysis (e.g., 415 K, 0.5–80 kPa CH_3OH or CH_3CH_2OH) [67,75,76].

Methanol dehydration proceeds through the concerted (i.e., associative) mechanism under relevant catalytic conditions (>4 kPa CH_3OH, 415 K) on all Al sites in CHA [75]. In this mechanism, methanol adsorbs to an H^+ site to form a bound methanol monomer, which then reacts with methanol to form a protonated methanol dimer that subsequently eliminates water and dimethyl ether (DME). Reaction orders are first- and zero-order in methanol pressure in the limiting cases of methanol monomer and dimer-covered sites, respectively. First-order methanol dehydration rate constants (415 K, per H^+), which reflect the energy to form the DME transition state relative to an adsorbed methanol monomer, are 7.2× higher on H^+ associated with 6-MR Al-Al site pairs in CHA than those associated with Al in other configurations (Fig. 2c), corresponding to a 7 kJ mol^{-1} lower ΔG_{act} value on 6-MR Al-Al site pairs [67]. Zero-order methanol dehydration rate constants (415 K, per H^+), which reflect the stability of the DME formation transition state relative to the protonated methanol dimer, are 4.4× higher on H^+ associated with 6-MR Al pairs, corresponding to a 5 kJ mol^{-1} lower ΔG_{act} value on 6-MR Al-Al site pairs [67]. DFT-computed Gibbs free energy barriers suggest that higher first- and zero-order rate constants for 6-MR Al-Al site pairs in CHA reflect the preferential stabilization of transition states over reactive intermediates via H-bonded networks with adsorbates at proximal acid sites [67].

Ethanol dehydration proceeds through a mechanism analogous to methanol dehydration [67]. First-order ethanol dehydration rate constants, which reflect the stability of the transition state to form diethyl ether (DEE) relative to a bound ethanol monomer, are 20× higher on H^+ sites associated with 6-MR Al-Al site pairs, corresponding to a 11 kJ mol^{-1} lower ΔG_{act} value on 6-MR Al-Al site pairs [67]. Zero-order ethanol dehydration rate constants, which reflect the stability of the DEE transition state relative to an adsorbed ethanol dimer, are also 20× higher on H^+ sites associated with 6-MR Al-Al site pairs (Fig. 2c), corresponding to a 10 kJ mol^{-1} lower ΔG_{act} value on 6-MR Al-Al site pairs [67]. These observations are rationalized by DFT-computed Gibbs free energy barriers that suggest extended H-bonded networks of co-adsorbed ethanol form on 6-MR Al-Al site pairs in CHA, analogous to those formed in methanol dehydration. Barriers for zeolite methylation were computed by DFT in the same study for 452 distinct Al arrangements in CHA with 1–5 Al per unit cell. Methylation barriers varied widely over different Al arrangements (by up to 114 kJ mol^{-1} among distinct configurations of 5 Al per unit cell) and were lowest for specific arrangements of Al that facilitated H-bonding interactions between the active Al center and a proximal spectating H^+ site. Notably, lower barriers did not correlate with a simple descriptor (e.g., H^+-H^+ distance) but depended on the specific orientation of both H^+ sites and, in turn, the specific Al arrangement. These findings illustrate the importance of developing quantitative characterization methods for distinct Al arrangements in zeolite frameworks and understanding the molecular interactions between proximal charge-compensating species and co-adsorbates to describe and predict catalytic function.

In contrast to alkanol dehydration, protolytic alkane cracking occurs at high temperatures (>673 K) at which H^+ sites are predominantly uncovered [45,77]. Protolytic propane cracking proceeds via protonation of a C-C bond to form an ion-pair transition state, which disso-

ciates to yield ethene and methane. First-order rate constants for protolytic propane cracking (748 K, per H^+) on H-CHA increased linearly with the fraction of 6-MR paired Al (0.00–0.44) [18]. First-order rate constants were 12× higher on H^+ associated with 6-MR Al-Al site pairs compared to H^+ associated with other arrangements of Al in CHA (Fig. 2d), corresponding to a 15 kJ mol^{-1} lower ΔG_{act} value on 6-MR Al-Al site pairs [18]. Although these differences may, in part, reflect changes in acid strength because protons are unoccupied during alkane activation catalysis, the nearly full and localized cationic charge (+0.9 e) [78-81] that develops at propane cracking transition states allows them to benefit similarly to protons as the conjugate base (i.e., deprotonated $[AlO_{4/2}]^-$) becomes more stable, thus attenuating the effects of changes in acid strength on apparent barriers [18,45,82]. Higher first-order rate constants on 6-MR Al pairs reflected less negative activation entropies for protolytic cracking on H^+ sites associated with those pairs (25 J mol^{-1} K^{-1}). Such entropic changes dominate Gibbs free energies at the high temperatures of this reaction [52]. More positive activation entropies on 6-MR paired Al sites in CHA were attributed to reflect later, more product-like, carbonium ion-like transition states at paired H^+ sites [18], as also proposed in an earlier report by Ding and co-workers for protolytic *n*-alkane cracking in MFI zeolites [17].

Alkanol dehydration and protolytic alkane cracking typify catalytic probe reactions that demonstrate the consequences of Al arrangements in CHA under very different catalytic conditions. Alkanol dehydration occurs under conditions of high coverage and low temperatures where the catalyst properties influencing activation enthalpies dominate changes in Gibbs free energy barriers. Transition states are enthalpically stabilized via H-bonding interactions with neighboring adsorbates bound to certain arrangements of proximal H^+ sites, resulting in lower Gibbs free energy barriers [67]. By contrast, protolytic alkane cracking occurs at high temperatures and under conditions of low coverage where the catalyst properties influencing activation entropies dominate changes to Gibbs free energy barriers. Under these conditions, 6-MR paired H^+ site arrangements appear to confer entropic benefits to protolytic alkane cracking transition states. These findings demonstrate the different mechanistic effects that become consequential for catalysis for different reaction mechanisms and temperatures, and illustrate that the distinct catalytic behavior of different proton site ensembles cannot be rationalized by a single mechanistic interpretation.

3. Characterization of Al arrangements in lower-symmetry zeolite frameworks

Exhaustive approaches to define and quantify catalytically relevant Al-Al arrangements are less tractable for low symmetry frameworks (e.g., FER, BEA, MFI) than for high-symmetry ones (e.g., CHA, FAU). The large combinatorial space of possible Al-Al pairs for low-symmetry structures impedes comprehensive assessments of Al arrangement models using computational approaches. Additionally, experimental attempts to quantify Al arrangements in low-symmetry frameworks are hindered by the dearth of methods to titrate distinct subsets of Al-Al site pairs in these frameworks. An important research direction, therefore, is the advancement of characterization methods and siting models for Al arrangements in low-symmetry zeolites. Our perspective is that the development of serviceable quantification methods for Al arrangements in low-symmetry zeolites and their connections to catalytic measurements can benefit from an analogous approach to that used to define Al-Al site pair ensembles in high-symmetry zeolites, but with consideration of the added complexity bestowed by the diversity of crystallographically unique T-sites present in low-symmetry frameworks. In this section, we focus on recent work that combines experiment and theory to develop quantitative Al-Al site pair models in MFI frameworks, as an illustrative example of how the conceptual framework developed for high-symmetry frameworks can be extended generally to low-symmetry frameworks.

3.1. Experimental and theoretical assessments of Al arrangement models in MFI frameworks

Although certain divalent cations (Cu^{2+}, Co^{2+}) are practical experimental probes of 6-MR paired Al in CHA, the extension of such an efficacious probe to MFI is not trivial given the additional void and ring structures that may alter the energetic landscape for divalent cation exchange. Several experimental techniques have been used to evaluate Al arrangements in MFI and other low-symmetry zeolites (e.g., MOR, FER) [83]. ^{29}Si MAS NMR has been used to quantify next-nearest neighbor pairs (Al-O-Si-O-Al), but cannot detect other Al-Al arrange-

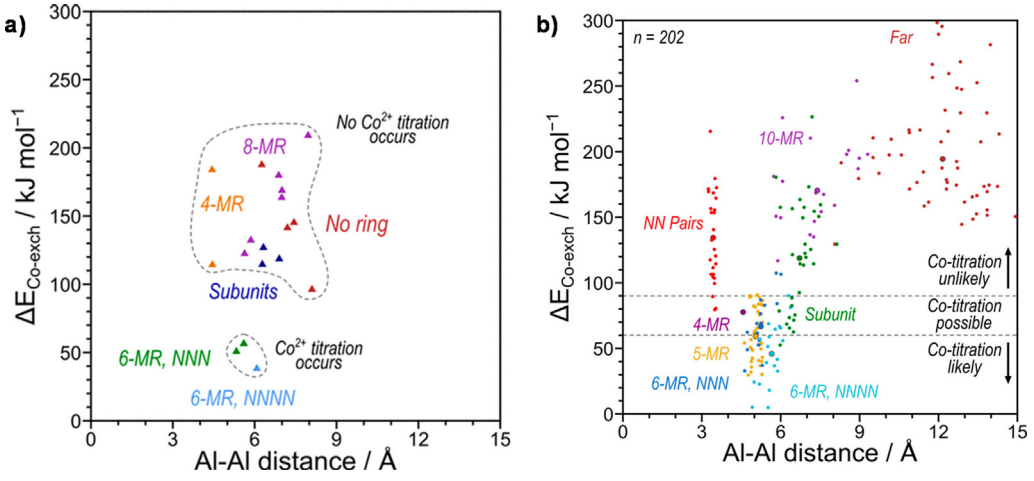

Fig. 3. Energy to exchange two protons for one Co^{2+} from $Co(NO_3)_2$ at (a) Al-Al pairs in CHA for pairs sharing 4-MR (orange), pairs sharing 6-MR and separated by 1 Si linker (6-MR NNN, green), pairs sharing 6-MR and separated by 2 Si linkers (6-MR NNNN, light blue), pairs sharing the di-6-MR and separated by 2Si linkers (subunit, navy), and pairs sharing larger 8-MR (purple), (b) Al-Al pairs in MFI. Distinct exchange locations in MFI are shown separately: Al in NN arrangements (red), Al-Al pair sharing a 4-MR (dark purple), 5-MR (yellow), or 6-MR and separated by 1 Si linker (6-MR NNN, dark blue) or by 2 Si linkers (6-MR NNNN, light blue), Al-Al pairs sharing MFI subunits but no ring (Subunit, green), Al–Al pairs sharing 10-MR (light purple), and Al-Al pairs sharing no ring (Far, brown). Larger dots show average values within each set. (For interpretation of the references to colour in this figure legend, the reader is referred to the web version of this article.). Figure reproduced from [88]

ments (e.g., next-next-nearest neighbor pairs). 2D ^{27}Al MAS NMR has been used to identify the T-sites in which Al is substituted, and to estimate the average number of Si separating two Al. This technique is non-quantitative and requires spectral deconvolution of many features whose chemical shifts depend on Al location and the number of Si separating two Al atoms [84]; however, higher resolution measurements can identify Al in distinct lattice positions in low-symmetry and partially-disordered frameworks (e.g., *SVY) [85].

Co^{2+} is widely used as a titrant of proximal Al sites in lower-symmetry frameworks because of the practical considerations mentioned in Section 2.1 [83,86,87]. As a result, several experimental characterization methods (e.g., DRUV–Vis) of Co-titrated MFI zeolites have been used to assess the Al-Al ensembles that may be present, however, these are subject to the same caveats that prevent accurate deconvolution and assignment of spectral features to specific X-MR binding sites. By contrast, theoretical calculations can more precisely assess the location and energies of Co^{2+} cations sited within different X-MR structures of MFI [88], as done for CHA. DFT-calculated Co^{2+} exchange energies at 202 distinct Al-Al arrangements considered to be plausible Co^{2+} binding sites (e.g., two Al within 7 Å or across an intersection) in an MFI unit cell (96 T-atoms) showed a wide range of Co^{2+} siting energies (5–300 kJ mol^{-1}, Fig. 3b). These Co^{2+} siting energies were compared to those in the 6-MR in CHA ($\Delta E_{Co\text{-}exch} \leq 50$ kJ mol^{-1}, Fig. 3a) and in other ring structures in CHA (4-, 8-MR) that are not titrated by Co^{2+} ($\Delta E_{Co\text{-}exch} > 100$ kJ mol^{-1}) to evaluate the Al-Al ensembles in MFI most likely to be titrated by Co^{2+}. Probable locations for Co^{2+} siting in MFI (0–100 kJ mol^{-1}) were predominantly (>85%) associated with Al-Al site pairs in 5- and 6-MRs, with a minority (<15%) of other possible binding sites consisting of Al-Al pairs in a 4-MR or two Al in two different subunit structures (Fig. 3b).

Experimental quantification of Al-Al site pairs in MFI via Co^{2+} exchange requires specific ion-exchange conditions that enable selective exchange of Co^{2+} and saturation of Al-Al site pairs, which can be verified through the measurement of an ion-exchange isotherm and quantitative characterization of the Co structures formed on the solid as discussed for CHA in Section 2.1. Notably, verification that Co^{2+} binding sites in MFI are saturated after aqueous ion exchange procedures (e.g., sequential ion-exchange at ambient temperature, or ion-exchange performed at higher temperatures such as 353 K [88]), is seldom performed, suggesting that many estimates of paired Al sites in MFI in literature reports are specious.

3.2. Synthesis of MFI zeolites with varied framework Al arrangement

The arrangement of framework Al in MFI zeolites varies with composition (Si/Al) and the SDAs used in synthesis. MFI crystallized with only tetrapropylammonium (TPA^+) contain four TPA^+ molecules occluded per unit cell (one per intersection) because the structure of TPA^+ restricts its occlusion to within MFI channel intersections. Consequently, up to four Al atoms may be sited (one per intersection; Si/Al = 23) in MFI crystallized with only TPA^+ as the charge-compensating SDA. MFI crystallized with only TPA^+ contained fractions of Co^{2+}-titratable Al pairs that increased (0–0.4) with increasing Al content as the Si/Al decreased (191–37) [88]. DFT energies were computed for 1773 distinct arrangements of two Al in an MFI unit cell (96 T-atoms) charge-compensated by two TPA^+ located in adjacent MFI intersections, for three distinct TPA^+-TPA^+ configurations. Energies of Al-Al arrangements charge-compensated by two TPA^+ cations in MFI were similar when separated by distances comparable to 6-MR Al-Al site pairs in CHA (5.1–6.0 Å) and in certain arrangements at longer distances (>6.0 Å; ~40 kJ mol^{-1}). These results suggest that Co^{2+}-titratable Al-Al site pair arrangements in MFI can be sited by two TPA^+ in neighboring intersections, which rationalizes the observation that Co^{2+}-titratable Al pairs are quantified experimentally in MFI samples crystallized using only TPA^+.

MFI zeolites were also crystallized with combinations of TPA^+ and a second, higher-charge-density inorganic SDA (Na^+) [88]. Addition of Na^+ ($\leq$3 Na^+/TPA^+) in MFI synthesis gels resulted in the occlusion of 1–2 Na^+ cations per unit cell (96 T-sites), but did not significantly affect the occlusion of TPA^+ cations (~4 per unit cell), suggesting these cationic SDAs can co-occlude in a cooperative manner. Both Na^+ and TPA^+ are capable of charge compensating a framework Al; however, MFI samples of fixed composition can be synthesized by fixing the total amount of cationic SDAs ((Na^++TPA^+)/Si). For MFI samples of essentially constant Si/Al (~50), the fraction of Co^{2+}-titratable Al pairs (0.1–0.5) generally increased with the occluded Na^+/TPA^+ ratio, and were higher than the fractions of Al pairs present when only TPA^+ was used as the SDA. MFI crystallized with Na^+ and a charge-neutral SDA (e.g., pentaerythritol) resulted in lower fractions of Al pairs at similar Al and Na^+ contents than samples crystallized using TPA^+ alone or using Na^+ and TPA^+ together. These findings suggest co-occlusion of cationic and neutral SDAs may form Al-Al arrangements that are not Co^{2+}-titratable (e.g., isolated Al) in MFI.

Arrangements of Al in MFI zeolites can also be influenced by co-incorporation of a second organic SDA (ethylenediamine, EDA) [89]. Synthesis of B-Al-MFI with TPA^+ resulted in the occlusion of one TPA^+ per intersection and the formation of a similar fraction of Co^{2+}-titratable Al pairs as in Al-MFI synthesized with only TPA^+. The fraction of Co^{2+}-titratable Al pairs was invariant with B content (Si/B (gel) = 2.5–500, Si/B (solid) = 48–340) [89]. Taken together, these observations suggest Co^{2+} selectively titrates Al-Al pairs in B-Al-MFI and that the arrangement of Al is not affected by the presence of B. The amount of TPA^+ occluded per unit cell decreased (4–1.4) when EDA was incorporated into MFI synthesis gels (EDA/TPA^+ = 1.0–3.8) suggesting that EDA competes with and displaces TPA^+ for occlusion within MFI voids [89]. It is possible that one or both amine groups in EDA (pKa ~ 10.7) [90] may become protonated under the basic conditions of synthesis (pH = 10–12); nonetheless, framework Al were charge-compensated by TPA^+ even when EDA was co-occluded, evident in TPA^+/Al ratios that remained constant near unity, irrespective of the occluded EDA content. Yet, B-Al-MFI synthesized with EDA and TPA^+ contained essentially only isolated Al ($\geq$ 95%) at all Al contents studied (Si/Al = 51–494), likely a consequence of the dilution of TPA^+ by co-occluded EDA that may have minimized TPA^+ occlusion in adjacent intersections. This demonstrates that the fraction of Co^{2+}-titratable Al achievable by one SDA can be altered by incorporation of a second SDA that competitively occludes within void spaces, and in a manner to allow synthesizing MFI with predominantly isolated Al.

3.3. Influence of Al arrangement in MFI zeolites on catalytic function

Alkanol dehydration and protolytic alkane cracking represent logical choices of reactions to probe the catalytic consequences of Al arrangement in MFI, given the distinct catalytic function of H^+ sites associated with Co^{2+}-titratable Al-Al site pair ensembles in CHA (i.e., 6-MR paired Al). First- and zero-order methanol dehydration rate constants have been reported by Jones et al. [91] for MFI samples obtained from commercial sources that vary in composition (Si/Al = 16–117) and Al arrangement, as other studies have measured fractions of Co^{2+}-titratable Al-Al pairs on these samples to vary from 0.08 to 0.58 [17,88]. First- and zero-order methanol dehydration rate constants (0.6–20 kPa CH_3OH, 433 K, per H^+) were similar for all but one H-MFI sample (Zeolyst, CBV3024E), suggesting a lack of correlation between

these rate constants and the fraction of Co^{2+}-titratable Al-Al pairs. This finding contrasts sharply the higher first- and zero-order methanol dehydration rate constants on 6-MR paired than isolated sites in H-CHA (by 7 × and 4×, respectively) under similar conditions (0.5–80 kPa CH_3OH, 415 K, per H^+), which originated from the formation of H-bonded networks of methanol clusters between adjacent H^+ sites in 6-MR Al-Al pairs in CHA. Structural differences between the MFI and CHA frameworks may preclude such H-bonded networks from forming within MFI. CHA is a small-pore zeolite with a window-cage structure, while MFI is a medium-pore zeolite with interconnecting straight and sinusoidal channels. The formation of methanol clusters at active sites in small-pore zeolites have been documented [75], but such effects have not been reported for medium- or large-pore zeolites. Topological differences among zeolites influence the conditions at which methanol clusters may begin to form, which may explain the weak influence of Co^{2+}-titratable Al pairs on methanol dehydration rate constants in H-MFI under the conditions studied.

In contrast to alkanol dehydration, Al arrangement has been proposed to influence protolytic alkane cracking in MFI [17,92] as well as CHA [18]. Song et al. measured propane, *n*-butane, and *n*-pentane cracking rate constants (per H^+) on H-MFI samples obtained from commercial sources (713–753 K, Si/Al = 15–140) and reported similar activation enthalpies but less negative activation entropies for samples with higher fractions of Co^{2+}-titratable Al-Al pairs, attributed to later and looser carbocationic transition states on paired H^+ sites [17]. Janda et al. studied *n*-butane cracking on commercial MFI samples, some of which were the same as those studied by Song et al. [17,92], and reported apparent entropies that generally became less negative with increasing fractions of Co^{2+}-titratable Al-Al pairs (723–788 K, Si/Al = 12–140) [92]. The authors attributed these entropic effects to larger fractions of Al located in channel intersections (~7 Å in diameter) as assessed through deconvolution of the DRUV–Vis d-d transition bands of Co^{2+}-exchanged zeolites, which were proposed to result in later and looser carbocationic transition states compared to those stabilized at Al in smaller channels (~5 Å in diameter). The differing interpretations of the two studies originate, in part, because of the non-rigorous identification of Co^{2+} locations from DRUV–Vis spectra (Section 2.1). Interestingly, the less negative apparent activation entropies measured on MFI with higher fractions of Co^{2+}-titratable Al in both studies are reminiscent of those measured on CHA samples with higher fractions of 6-MR pairs [18], suggesting the mechanistic influence of proton pairs on protolytic alkane cracking catalysis may be generalizable among zeolite frameworks.

4. Outlook

The catalytic diversity of proton active sites in different void locations or relative proximity within aluminosilicate zeolites is elucidated by interrogating materials of fixed composition, where such effects are eminently recognizable. This approach facilitates the development of quantitative synthesis-structure–function relations for zeolites that incorporate the effects of Al arrangement. Mechanistic connections among the three components of a synthesis-structure–function relation strengthen their utility, but are predicated on quantitative methods to characterize distinct Al-Al site ensembles and to measure their catalytic reactivity, and synthetic or post-synthetic methods to form such ensembles in zeolitic frameworks.

Current efforts to quantify distinct Al-Al site ensembles in zeolites are challenged by a dearth of characterization methods. Titrating subsets of Al-Al site pairs using divalent cations, and identifying their probable binding sites using experimental and theoretical assessments, is a useful approach. We have demonstrated this approach in the case of Co^{2+}, which selectively titrates Al-Al site pairs in the 6-MR of CHA and a broader swath of Al-Al site pairs in 5- and 6-MRs of MFI. Divalent cations of different size should titrate Al-Al site pair ensembles separated by different distances or within different X-MRs (e.g., Al-Al pairs in the 8-MR of CHA), allowing for experimental quantification of different subsets of Al-Al site pairs with the concomitant guidance provided by DFT-estimated cation binding energies at various X-MRs [58]. Another strategy is to identify Al-Al site pairs that preferentially bind specific intermediates or transition states in a chemical reaction, for which the length scale between adjacent proton sites may be more appropriately probed using a titrant molecule that serves as a surrogate for the kinetically-relevant intermediates and transition states. One recent example is the use of IR spectroscopy to monitor features arising from distinct types of propene interactions with K^+ cations exchanged at proximal and isolated Al sites in FER zeolites [93], which may be relevant for interpreting the influence of acid site proximity on propene reactions (e.g., oligomerization). Furthermore, divalent cation titrations characterize Al arrangements present throughout zeolitic materials and are thus insensitive to structural heterogeneities that often exist (e.g., Al zoning, polydisperse crystal size or morphology [10,94]), motivating the development of characterization tools that quantify Al arrangements and are sensitive to spatial heterogeneities that exist within a given sample (e.g., XPS [95], SEM-EDX [96], TEM-EDX [65]).

Unambiguous assessments of acid site proximity effects on catalytic function first require a detailed mechanistic understanding of the reaction. We have illustrated this using alkanol dehydration and alkane cracking as examples wherein higher turnover rates at 6-MR paired than isolated sites in CHA reflect distinct mechanistic effects. As a result, there is no single mechanism by which proximal protons influence rates of acid-catalyzed reactions, precluding generalization across reaction mechanisms, or even for a given reaction across varying reaction conditions that change the kinetic relevance of specific intermediates or elementary steps. For the reaction under study, direct experimental measurements of rate constants requires that corruptions from heat or mass transport phenomena are absent, and that turnover rates are normalized by the number of putative active site ensembles [41]. More direct mechanistic links between structure and function are possible when catalytic behavior is quantified in the form of rate constants, rather than measurements of probe reactions that only provide inferences of rate constants (e.g., constraint index or "alpha" tests) and may also reflect catalyst properties other than active site arrangement.

Finally, the often-neglected aspect of any structure–function relation is the ability to synthesize materials comprising wide variations in the structural property of interest, which helps ensure that the relation identified will apply broadly to a family of materials rather than just the samples under interrogation. Synthetic protocols to vary Al siting and arrangement in zeolite frameworks include using different monovalent and divalent [97] SDAs (and combinations thereof) during crystallization from amorphous precursors, and alternate crystallization routes involving the disassembly of partially- or fully-constituted zeolitic domains [98,99]. Additionally, computational modeling can accelerate experimental materials design and discovery efforts by modeling SDA-framework interactions to determine how SDAs (and combinations thereof) may energetically favor the formation of certain framework topologies [100-102] and Al arrangements [58]. Computational predictions also suggest energetically preferred Al arrangements in H-form zeolites that violate Löwenstein's rule (i.e., Al in nearest neighbor locations) [103-106]. Given that zeolites cannot be crystallized directly in the proton-form, different Al arrangements

may be accessible via post-synthetic modification of framework bonds in H-form zeolites, which can occur at ambient temperatures in liquid water (e.g., $H_2^{17}O$) to cause ^{17}O isotopic enrichment of the lattice detectable by ^{17}O NMR [107], and perhaps even at high-temperatures during steam treatments as inferred by observations of changing structures of exchanged cations (e.g., Cu^{2+}) [108,109]. Recent work on the interzeolite conversion of FAU to MFI in the presence of organic and inorganic SDAs (TPA^+, Na^+) has shown that the fraction of Co^{2+}-titratable Al systematically decreased (0.20–0.05) with increasing time (2–128 h), suggesting that framework Al rearrange under the conditions of hydrothermal synthesis [65]. Thus, a combination of kinetic and thermodynamic factors influence the Al arrangements that form in zeolite frameworks, providing many strategies to prepare materials containing different numbers and types of Al-Al site pair ensembles.

In conclusion, different arrangements of Al heteroatoms in zeolite frameworks influence the structure and stability of reactive intermediates and transition states in acid catalysis, and the binding of molecules in various adsorption and separation applications [110,111], further broadening the functional diversity of aluminosilicate zeolites and providing one of the only options to do so among materials of fixed bulk structure and composition. Given the challenges associated with precisely defining Al arrangements in zeolites in each component of a synthesis-structure–function relation, the discordant interpretations and conclusions among literature reports regarding the catalytic consequences of proton site arrangements in Brønsted acid catalysis are perhaps unsurprising. The development of methods to more precisely quantify distinct site pair ensembles in zeolites is foundational to unambiguously determining their consequences for catalysis, and to designing synthetic and post-synthetic routes to predictably alter active site arrangements, in order to realize the full potential of the catalytic diversity of aluminosilicate zeolites.

Declaration of Competing Interest

The authors declare that they have no known competing financial interests or personal relationships that could have appeared to influence the work reported in this paper.

Acknowledgements

We acknowledge financial support by the National Science Foundation DMREF program (1922173-CBET). We thank John R. Di Iorio, Philip M. Kester, Dr. Young Gul Hur, and ByungJin Lee for helpful technical discussions, and Dr. Songhyun Lee for a critical proofreading of this manuscript. We also acknowledge with thanks the many helpful technical discussions with Alexander J. Hoffman and Prof. David D. Hibbitts (University of Florida), Jerry T. Crum, Yujia Wang, and Prof. William F. Schneider (University of Notre Dame), and Ahmad Moini, Subramanian Prasad and Anthony DeBellis and their research groups at BASF Corporation.

References

[1] P.B. Venuto, Organic catalysis over zeolites: A perspective on reaction paths within micropores, Microporous Materials. 2 (1994) 297–411, https://doi.org/10.1016/0927-6513(94)00002-6.
[2] A. Corma, Inorganic Solid Acids and Their Use in Acid-Catalyzed Hydrocarbon Reactions, Chem. Rev. 95 (1995) 559–614, https://doi.org/10.1021/cr00035a006.
[3] R.J. Gorte, S.P. Crossley, A perspective on catalysis in solid acids, Journal of Catalysis. 375 (2019) 524–530, https://doi.org/10.1016/j.jcat.2019.07.015.
[4] E. Haldoupis, S. Nair, D.S. Sholl, Pore size analysis of >250 000 hypothetical zeolites, Phys. Chem. Chem. Phys. 13 (2011) 5053–5060, https://doi.org/10.1039/C0CP02766A.
[5] E.L. First, C.E. Gounaris, J. Wei, C.A. Floudas, Computational characterization of zeolite porous networks: an automated approach, Phys. Chem. Chem. Phys. 13 (2011) 17339–17358, https://doi.org/10.1039/C1CP21731C.
[6] T.F. Degnan, The implications of the fundamentals of shape selectivity for the development of catalysts for the petroleum and petrochemical industries, Journal of Catalysis. 216 (2003) 32–46, https://doi.org/10.1016/S0021-9517(02)00105-7.
[7] S.M. Csicsery, Shape-selective catalysis in zeolites, Zeolites. 4 (1984) 202–213, https://doi.org/10.1016/0144-2449(84)90024-1.
[8] W.O. Haag, R.M. Lago, P.B. Weisz, The active site of acidic aluminosilicate catalysts, Nature. 309 (1984) 589–591, https://doi.org/10.1038/309589a0.
[9] W.O. Haag, Catalysis by Zeolites – Science and Technology, in: J. Weitkamp, H.G. Karge, H. Pfeifer, W. Hölderich (Eds.), Studies in Surface Science and Catalysis, Elsevier, 1994, pp. 1375–1394, https://doi.org/10.1016/S0167-2991(08)63680-0.
[10] T.T. Le, A. Chawla, J.D. Rimer, Impact of acid site speciation and spatial gradients on zeolite catalysis, Journal of Catalysis. 391 (2020) 56–68, https://doi.org/10.1016/j.jcat.2020.08.008.
[11] A.B. Pinar, R. García, L. Gómez-Hortigüela, J. Pérez-Pariente, Synthesis of Open Zeolite Structures from Mixtures of Tetramethylammonium and Benzylmethylalkylammonium Cations: A Step Towards Driving Aluminium Location in the Framework, Top Catal. 53 (2010) 1297–1303, https://doi.org/10.1007/s11244-010-9587-4.
[12] A.B. Pinar, L. Gomez-Hortiguela, J. Perez-Pariente, Cooperative Structure Directing Role of the Cage-Forming Tetramethylammonium Cation and the Bulkier Benzylmethylpyrrolidinium in the Synthesis of Zeolite Ferrierite, Chem. Mater. 19 (2007) 5617–5626, https://doi.org/10.1021/cm071753o.
[13] B.C. Knott, C.T. Nimlos, D.J. Robichaud, M.R. Nimlos, S. Kim, R. Gounder, Consideration of the Aluminum Distribution in Zeolites in Theoretical and Experimental Catalysis Research, ACS Catal. 8 (2018) 770–784, https://doi.org/10.1021/acscatal.7b03676.
[14] J. Dědeček, Z. Sobalík, B. Wichterlová, Siting and Distribution of Framework Aluminium Atoms in Silicon-Rich Zeolites and Impact on Catalysis, Catalysis Reviews. 54 (2012) 135–223, https://doi.org/10.1080/01614940.2012.632662.
[15] S.P. Crossley, D.E. Resasco, G.L. Haller, Clarifying the multiple roles of confinement in zeolites: From stabilization of transition states to modification of internal diffusion rates, Journal of Catalysis. 372 (2019) 382–387, https://doi.org/10.1016/j.jcat.2019.03.010.
[16] R. Gounder, E. Iglesia, The catalytic diversity of zeolites: confinement and solvation effects within voids of molecular dimensions, Chem. Commun. 49 (2013) 3491–3509, https://doi.org/10.1039/C3CC40731D.
[17] C. Song, Y. Chu, M. Wang, H. Shi, L. Zhao, X. Guo, W. Yang, J. Shen, N. Xue, L. Peng, W. Ding, Cooperativity of adjacent Brønsted acid sites in MFI zeolite channel leads to enhanced polarization and cracking of alkanes, Journal of Catalysis. 349 (2017) 163–174, https://doi.org/10.1016/j.jcat.2016.12.024.
[18] P.M. Kester, J.T. Crum, S. Li, W.F. Schneider, R. Gounder, Effects of Brønsted Acid Site Proximity in Chabazite Zeolites on OH Infrared Spectra and Protolytic Propane Cracking Kinetics, Journal of Catalysis. (2021), https://doi.org/10.1016/j.jcat.2020.12.038.
[19] A.N. Mlinar, P.M. Zimmerman, F.E. Celik, M. Head-Gordon, A.T. Bell, Effects of Brønsted-acid site proximity on the oligomerization of propene in H-MFI, Journal of Catalysis. 288 (2012) 65–73, https://doi.org/10.1016/j.jcat.2012.01.002.
[20] M. Bernauer, E. Tabor, V. Pashkova, D. Kaucký, Z. Sobalík, B. Wichterlová, J. Dedecek, Proton proximity – New key parameter controlling adsorption, desorption and activity in propene oligomerization over H-ZSM-5 zeolites, Journal of Catalysis. 344 (2016) 157–172, https://doi.org/10.1016/j.jcat.2016.09.025.
[21] E.M. Gallego, C. Li, C. Paris, N. Martín, J. Martínez-Triguero, M. Boronat, M. Moliner, A. Corma, Making Nanosized CHA Zeolites with Controlled Al Distribution for Optimizing Methanol-to-Olefin Performance, Chemistry – A, European Journal. 24 (2018) 14631–14635, https://doi.org/10.1002/chem.201803637.
[22] M.A. Deimund, L. Harrison, J.D. Lunn, Y. Liu, A. Malek, R. Shayib, M.E. Davis, Effect of Heteroatom Concentration in SSZ-13 on the Methanol-to-Olefins Reaction, ACS Catal. 6 (2016) 542–550, https://doi.org/10.1021/acscatal.5b01450.
[23] M.J. Wulfers, S. Teketel, B. Ipek, R.F. Lobo, Conversion of methane to methanol on copper-containing small-pore zeolites and zeotypes, Chem. Commun. 51 (2015) 4447–4450, https://doi.org/10.1039/C4CC09645B.

[24] P.J. Smeets, M.H. Groothaert, R.A. Schoonheydt, Cu based zeolites: A UV–vis study of the active site in the selective methane oxidation at low temperatures, Catalysis Today. 110 (2005) 303–309, https://doi.org/10.1016/j.cattod.2005.09.028.
[25] J. Devos, M.L. Bols, D. Plessers, C.V. Goethem, J.W. Seo, S.-J. Hwang, B.F. Sels, M. Dusselier, Synthesis–Structure–Activity Relations in Fe-CHA for C-H Activation: Control of Al Distribution by Interzeolite Conversion, Chem. Mater. 32 (2020) 273–285, https://doi.org/10.1021/acs.chemmater.9b03738.
[26] S. Li, Y. Wang, T. Wu, W.F. Schneider, First-Principles Analysis of Site- and Condition-Dependent Fe Speciation in SSZ-13 and Implications for Catalyst Optimization, ACS Catal. 8 (2018) 10119–10130, https://doi.org/10.1021/acscatal.8b02107.
[27] J. Gao, Y. Zheng, J.-M. Jehng, Y. Tang, I.E. Wachs, S.G. Podkolzin, Identification of molybdenum oxide nanostructures on zeolites for natural gas conversion, Science. 348 (2015) 686–690, https://doi.org/10.1126/science.aaa7048.
[28] J. Gao, Y. Zheng, G.B. Fitzgerald, J. de Joannis, Y. Tang, I.E. Wachs, S.G. Podkolzin, Structure of Mo2Cx and Mo4Cx Molybdenum Carbide Nanoparticles and Their Anchoring Sites on ZSM-5 Zeolites, J. Phys. Chem. C. 118 (2014) 4670–4679, https://doi.org/10.1021/jp4106053.
[29] N.K. Razdan, A. Kumar, B.L. Foley, A. Bhan, Influence of ethylene and acetylene on the rate and reversibility of methane dehydroaromatization on Mo/H-ZSM-5 catalysts, Journal of Catalysis. 381 (2020) 261–270, https://doi.org/10.1016/j.jcat.2019.11.004.
[30] N.M. Phadke, J. Van der Mynsbrugge, E. Mansoor, A.B. Getsoian, M. Head-Gordon, A.T. Bell, Characterization of Isolated Ga3+ Cations in Ga/H-MFI Prepared by Vapor-Phase Exchange of H-MFI Zeolite with GaCl3, ACS Catal. 8 (2018) 6106–6126, https://doi.org/10.1021/acscatal.8b01254.
[31] N.M. Phadke, E. Mansoor, M. Bondil, M. Head-Gordon, A.T. Bell, Mechanism and Kinetics of Propane Dehydrogenation and Cracking over Ga/H-MFI Prepared via Vapor-Phase Exchange of H-MFI with GaCl3, J. Am. Chem. Soc. 141 (2019) 1614–1627, https://doi.org/10.1021/jacs.8b11443.
[32] M.W. Schreiber, C.P. Plaisance, M. Baumgärtl, K. Reuter, A. Jentys, R. Bermejo-Deval, J.A. Lercher, Lewis-Brønsted Acid Pairs in Ga/H-ZSM-5 To Catalyze Dehydrogenation of Light Alkanes, J. Am. Chem. Soc. 140 (2018) 4849–4859, https://doi.org/10.1021/jacs.7b12901.
[33] M.H. Groothaert, K. Lievens, J.A. van Bokhoven, A.A. Battiston, B.M. Weckhuysen, K. Pierloot, R.A. Schoonheydt, Bis(μ-OXO)dicopper as intermediate in the catalytic decomposition of No over Cu-ZSM-5, in: E. van Steen, M. Claeys, L.H. Callanan (Eds.), Studies in Surface Science and Catalysis, Elsevier, 2004, pp. 2449–2457, https://doi.org/10.1016/S0167-2991(04)80510-X.
[34] F. Giordanino, P.N.R. Vennestrøm, L.F. Lundegaard, F.N. Stappen, S. Mossin, P. Beato, S. Bordiga, C. Lamberti, Characterization of Cu-exchanged SSZ-13: a comparative FTIR, UV-Vis, and EPR study with Cu-ZSM-5 and Cu-β with similar Si/Al and Cu/Al ratios, Dalton Trans. 42 (2013) 12741–12761, https://doi.org/10.1039/C3DT50732G.
[35] C. Paolucci, A.A. Parekh, I. Khurana, J.R. Di Iorio, H. Li, J.D. Albarracin Caballero, A.J. Shih, T. Anggara, W.N. Delgass, J.T. Miller, F.H. Ribeiro, R. Gounder, W.F. Schneider, Catalysis in a Cage: Condition-Dependent Speciation and Dynamics of Exchanged Cu Cations in SSZ-13 Zeolites, J. Am. Chem. Soc. 138 (2016) 6028–6048, https://doi.org/10.1021/jacs.6b02651.
[36] P. Sazama, B. Wichterlová, E. Tábor, P. Šťastný, N.K. Sathu, Z. Sobalík, J. Dědeček, Š. Sklenák, P. Klein, A. Vondrová, Tailoring of the structure of Fe-cationic species in Fe-ZSM-5 by distribution of Al atoms in the framework for N2O decomposition and NH3-SCR-NOx, Journal of Catalysis. 312 (2014) 123–138, https://doi.org/10.1016/j.jcat.2014.01.019.
[37] N. Hansen, A. Heyden, A.T. Bell, F.J. Keil, A Reaction Mechanism for the Nitrous Oxide Decomposition on Binuclear Oxygen Bridged Iron Sites in Fe-ZSM-5, J. Phys. Chem. C. 111 (2007) 2092–2101, https://doi.org/10.1021/jp065574q.
[38] S. Sklenak, P.C. Andrikopoulos, B. Boekfa, B. Jansang, J. Nováková, L. Benco, T. Bucko, J. Hafner, J. Dědeček, Z. Sobalík, N2O decomposition over Fe-zeolites: Structure of the active sites and the origin of the distinct reactivity of Fe-ferrierite, Fe-ZSM-5, and Fe-beta. A combined periodic DFT and multispectral study, Journal of Catalysis. 272 (2010) 262–274, https://doi.org/10.1016/j.jcat.2010.04.008.
[39] Z. Sobalik, P. Sazama, J. Dedecek, B. Wichterlová, Critical evaluation of the role of the distribution of Al atoms in the framework for the activity of metallo-zeolites in redox N2O/NOx reactions, Applied Catalysis A: General. 474 (2014) 178–185, https://doi.org/10.1016/j.apcata.2013.07.033.
[40] B.R. Goodman, K.C. Hass, W.F. Schneider, J.B. Adams, Statistical analysis of Al distributions and metal ion pairing probabilities in zeolites, Catalysis Letters. 68 (2000) 85–93, https://doi.org/10.1023/A:1019066916541.
[41] M. Boudart, Turnover Rates in Heterogeneous Catalysis, Chem. Rev. 95 (1995) 661–666, https://doi.org/10.1021/cr00035a009.
[42] A.J. Jones, E. Iglesia, The Strength of Brønsted Acid Sites in Microporous Aluminosilicates, ACS Catal. 5 (2015) 5741–5755, https://doi.org/10.1021/acscatal.5b01133.
[43] A. Bhan, A.D. Allian, G.J. Sunley, D.J. Law, E. Iglesia, Specificity of Sites within Eight-Membered Ring Zeolite Channels for Carbonylation of Methyls to Acetyls, J. Am. Chem. Soc. 129 (2007) 4919–4924, https://doi.org/10.1021/ja070094d.
[44] R. Gounder, E. Iglesia, Effects of Partial Confinement on the Specificity of Monomolecular Alkane Reactions for Acid Sites in Side Pockets of Mordenite, Angewandte Chemie International Edition. 49 (2010) 808–811, https://doi.org/10.1002/anie.200905869.
[45] R. Gounder, E. Iglesia, Catalytic Consequences of Spatial Constraints and Acid Site Location for Monomolecular Alkane Activation on Zeolites, J. Am. Chem. Soc. 131 (2009) 1958–1971, https://doi.org/10.1021/ja808292c.
[46] R. Gounder, E. Iglesia, Catalytic hydrogenation of alkenes on acidic zeolites: Mechanistic connections to monomolecular alkane dehydrogenation reactions, Journal of Catalysis. 277 (2011) 36–45, https://doi.org/10.1016/j.jcat.2010.10.013.
[47] R. Gounder, E. Iglesia, Catalytic Alkylation Routes via Carbonium-Ion-Like Transition States on Acidic Zeolites, ChemCatChem. 3 (2011) 1134–1138, https://doi.org/10.1002/cctc.201100051.
[48] M.L. Sarazen, E. Doskocil, E. Iglesia, Effects of Void Environment and Acid Strength on Alkene Oligomerization Selectivity, ACS Catal. 6 (2016) 7059–7070, https://doi.org/10.1021/acscatal.6b02128.
[49] R.T. Carr, M. Neurock, E. Iglesia, Catalytic consequences of acid strength in the conversion of methanol to dimethyl ether, Journal of Catalysis. 278 (2011) 78–93, https://doi.org/10.1016/j.jcat.2010.11.017.
[50] A.J. Jones, S.I. Zones, E. Iglesia, Implications of Transition State Confinement within Small Voids for Acid Catalysis, The Journal of Physical Chemistry C. 118 (2014) 17787–17800, https://doi.org/10.1021/jp5050095.
[51] S. Herrmann, E. Iglesia, Elementary steps in acetone condensation reactions catalyzed by aluminosilicates with diverse void structures, Journal of Catalysis. 346 (2017) 134–153, https://doi.org/10.1016/j.jcat.2016.12.011.
[52] R. Gounder, E. Iglesia, The Roles of Entropy and Enthalpy in Stabilizing Ion-Pairs at Transition States in Zeolite Acid Catalysis, Acc. Chem. Res. 45 (2012) 229–238, https://doi.org/10.1021/ar200138n.
[53] A. Bhan, E. Iglesia, A Link between Reactivity and Local Structure in Acid Catalysis on Zeolites, Acc. Chem. Res. 41 (2008) 559–567, https://doi.org/10.1021/ar700181t.
[54] C. Baerlocher, L.B. McCusker, Database of Zeolite Structures, (n.d.). http://www.iza-structure.org/databases/ (accessed February 14, 2021).
[55] W. Loewenstein, The distribution of aluminum in the tetrahedra of silicates and aluminates, American Mineralogist. 39 (1954) 92–96.
[56] S.A. Bates, A.A. Verma, C. Paolucci, A.A. Parekh, T. Anggara, A. Yezerets, W.F. Schneider, J.T. Miller, W.N. Delgass, F.H. Ribeiro, Identification of the active Cu site in standard selective catalytic reduction with ammonia on Cu-SSZ-13, Journal of Catalysis. 312 (2014) 87–97, https://doi.org/10.1016/j.jcat.2014.01.004.
[57] J.R. Di Iorio, R. Gounder, Controlling the Isolation and Pairing of Aluminum in Chabazite Zeolites Using Mixtures of Organic and Inorganic Structure-Directing Agents, Chem. Mater. 28 (2016) 2236–2247, https://doi.org/10.1021/acs.chemmater.6b00181.
[58] J.R. Di Iorio, S. Li, C.B. Jones, C.T. Nimlos, Y. Wang, E. Kunkes, V. Vattipalli, S. Prasad, A. Moini, W.F. Schneider, R. Gounder, Cooperative and Competitive Occlusion of Organic and Inorganic Structure-Directing Agents within Chabazite Zeolites Influences Their Aluminum Arrangement, J. Am. Chem. Soc. 142 (2020) 4807–4819, https://doi.org/10.1021/jacs.9b13817.
[59] M. Pourbaix, Atlas of electrochemical equilibria in aqueous solutions, National Association of Corrosion Engineers, Houston, Tex., 1974.
[60] H. Li, C. Paolucci, I. Khurana, L.N. Wilcox, F. Göltl, J.D. Albarracin-Caballero, A.J. Shih, F.H. Ribeiro, R. Gounder, W.F. Schneider, Consequences of exchange-site heterogeneity and dynamics on the UV-visible spectrum of Cu-exchanged SSZ-13, Chem. Sci. 10 (2019) 2373–2384, https://doi.org/10.1039/C8SC05056B.
[61] T. Montanari, M. Bevilacqua, C. Resini, G. Busca, UV−Vis and FT-IR Study of the Nature and Location of the Active Sites of Partially Exchanged Co−H Zeolites, J. Phys. Chem. B. 108 (2004) 2120–2127, https://doi.org/10.1021/jp034814o.
[62] L.F. Liotta, G. Pantaleo, A. Macaluso, G. Di Carlo, G. Deganello, CoOx catalysts supported on alumina and alumina-baria: influence of the support on the cobalt species and their activity in NO reduction by C3H6 in lean conditions, Applied Catalysis A: General. 245 (2003) 167–177, https://doi.org/10.1016/S0926-860X(02)00652-X.
[63] P.V. Radovanovic, N.S. Norberg, K.E. McNally, D.R. Gamelin, Colloidal Transition-Metal-Doped ZnO Quantum Dots, J. Am. Chem. Soc. 124 (2002) 15192–15193, https://doi.org/10.1021/ja028416v.
[64] A. Bellmann, C. Rautenberg, U. Bentrup, A. Brückner, Determining the Location of Co2+ in Zeolites by UV-Vis Diffuse Reflection Spectroscopy: A Critical View, Catalysts. 10 (2020) 123, https://doi.org/10.3390/catal10010123.
[65] J. Devos, S. Robijns, C. Van Goethem, I. Khalil, M. Dusselier, Interzeolite Conversion and the Role of Aluminum: Toward Generic Principles of Acid Site Genesis and Distributions in ZSM-5 and SSZ-13, Chem. Mater. (2021), https://doi.org/10.1021/acs.chemmater.0c04832.
[66] K. Chen, M. Abdolrahmani, S. Horstmeier, T.N. Pham, V.T. Nguyen, M. Zeets, B. Wang, S. Crossley, J.L. White, Brønsted-Brønsted Synergies between Framework and Noncrystalline Protons in Zeolite H-ZSM-5, ACS Catal. 9 (2019) 6124–6136, https://doi.org/10.1021/acscatal.9b01583.

[67] A.J. Hoffman, J.S. Bates, J.R.D. Iorio, S.V. Nystrom, C.T. Nimlos, R. Gounder, D. Hibbitts, Rigid Arrangements of Ionic Charge in Zeolite Frameworks Conferred by Specific Aluminum Distributions Preferentially Stabilize Alkanol Dehydration Transition States, Angewandte Chemie International Edition. 59 (2020) 18686–18694, https://doi.org/10.1002/anie.202007790.
[68] W. Lv, S. Wang, P. Wang, Y. Liu, Z. Huang, J. Li, M. Dong, J. Wang, W. Fan, Regulation of Al distributions and Cu2+ locations in SSZ-13 zeolites for NH3-SCR of NO by different alkali metal cations, Journal of Catalysis. 393 (2021) 190–201, https://doi.org/10.1016/j.jcat.2020.11.027.
[69] Y. Liang, A.J. Jacobson, J.D. Rimer, Strontium Ions Function as Both an Accelerant and Structure-Directing Agent of Chabazite Crystallization, ACS Materials Lett. (2020) 187–192, https://doi.org/10.1021/acsmaterialslett.0c00460.
[70] T. Nishitoba, N. Yoshida, J.N. Kondo, T. Yokoi, Control of Al Distribution in the CHA-Type Aluminosilicate Zeolites and Its Impact on the Hydrothermal Stability and Catalytic Properties, Ind. Eng. Chem. Res. 57 (2018) 3914–3922, https://doi.org/10.1021/acs.iecr.7b04985.
[71] K. Muraoka, Y. Sada, A. Shimojima, W. Chaikittisilp, T. Okubo, Tracking the rearrangement of atomic configurations during the conversion of FAU zeolite to CHA zeolite, Chem. Sci. 10 (2019) 8533–8540, https://doi.org/10.1039/C9SC02773D.
[72] Y. Ji, M.A. Deimund, Y. Bhawe, M.E. Davis, Organic-Free Synthesis of CHA-Type Zeolite Catalysts for the Methanol-to-Olefins Reaction, ACS Catal. 5 (2015) 4456–4465, https://doi.org/10.1021/acscatal.5b00404.
[73] K. Mlekodaj, M. Bernauer, J.E. Olszowka, P. Klein, V. Pashkova, J. Dedecek, Synthesis of the Zeolites from SBU: An SSZ-13 Study acs.chemmater.0c04710 Chem. Mater. (2021), https://doi.org/10.1021/acs.chemmater.0c04710.
[74] S. Nystrom, A. Hoffman, D. Hibbitts, Tuning Brønsted Acid Strength by Altering Site Proximity in CHA Framework Zeolites, ACS Catal. 8 (2018) 7842–7860, https://doi.org/10.1021/acscatal.8b02049.
[75] J.R. Di Iorio, A.J. Hoffman, C.T. Nimlos, S. Nystrom, D. Hibbitts, R. Gounder, Mechanistic origins of the high-pressure inhibition of methanol dehydration rates in small-pore acidic zeolites, Journal of Catalysis. 380 (2019) 161–177, https://doi.org/10.1016/j.jcat.2019.10.012.
[76] J.R. Di Iorio, C.T. Nimlos, R. Gounder, Introducing Catalytic Diversity into Single-Site Chabazite Zeolites of Fixed Composition via Synthetic Control of Active Site Proximity, ACS Catal. 7 (2017) 6663–6674, https://doi.org/10.1021/acscatal.7b01273.
[77] H. Li, S.A. Kadam, A. Vimont, R.F. Wormsbecher, A. Travert, Monomolecular Cracking Rates of Light Alkanes over Zeolites Determined by IR Operando Spectroscopy, ACS Catal. 6 (2016) 4536–4548, https://doi.org/10.1021/acscatal.6b01025.
[78] R.A. van Santen, G.J. Kramer, Reactivity Theory of Zeolitic Broensted Acidic Sites, Chem. Rev. 95 (1995) 637–660, https://doi.org/10.1021/cr00035a008.
[79] A.M. Rigby, G.J. Kramer, R.A. van Santen, Mechanisms of Hydrocarbon Conversion in Zeolites: A Quantum Mechanical Study, Journal of Catalysis. 170 (1997) 1–10, https://doi.org/10.1006/jcat.1997.1574.
[80] M.V. Frash, R.A. van Santen, Quantum-chemical modeling of the hydrocarbon transformations in acid zeolite catalysts, Topics in Catalysis. 9 (1999) 191–205, https://doi.org/10.1023/A:1019183110705.
[81] S.A. Zygmunt, L.A. Curtiss, P. Zapol, L.E. Iton, Ab Initio and Density Functional Study of the Activation Barrier for Ethane Cracking in Cluster Models of Zeolite H-ZSM-5, J. Phys. Chem. B. 104 (2000) 1944–1949, https://doi.org/10.1021/jp993194h.
[82] P. Deshlahra, R.T. Carr, E. Iglesia, Ionic and Covalent Stabilization of Intermediates and Transition States in Catalysis by Solid Acids, J. Am. Chem. Soc. 136 (2014) 15229–15247, https://doi.org/10.1021/ja506149c.
[83] J. Dêdeĉek, V. Gábová, B. Wichterlová, The effect of dealumination on the Al distribution in pentasil ring zeolites, in: R. Aiello, G. Giordano, F. Testa (Eds.), Studies in Surface Science and Catalysis, Elsevier, 2002, pp. 1817–1824, https://doi.org/10.1016/S0167-2991(02)80357-3.
[84] J. Dědeček, S. Sklenak, C. Li, B. Wichterlová, V. Gábová, J. Brus, M. Sierka, J. Sauer, Effect of Al−Si−Al and Al−Si−Si−Al Pairs in the ZSM-5 Zeolite Framework on the 27Al NMR Spectra. A Combined High-Resolution 27Al NMR and DFT/MM Study, J. Phys. Chem. C. 113 (2009) 1447–1458. https://doi.org/10.1021/jp8068333.
[85] Z.J. Berkson, M.-F. Hsieh, S. Smeets, D. Gajan, A. Lund, A. Lesage, D. Xie, S.I. Zones, L.B. McCusker, C. Baerlocher, B.F. Chmelka, Preferential Siting of Aluminum Heteroatoms in the Zeolite Catalyst Al-SSZ-70, Angewandte Chemie. 131 (2019) 6321–6325, https://doi.org/10.1002/ange.201813533.
[86] K. Klier, Transition-metal ions in zeolites: the perfect surface sites, Langmuir. 4 (1988) 13–25, https://doi.org/10.1021/la00079a003.
[87] J. Dedecek, V. Balgová, V. Pashkova, P. Klein, B. Wichterlová, Synthesis of ZSM-5 Zeolites with Defined Distribution of Al Atoms in the Framework and Multinuclear MAS NMR Analysis of the Control of Al Distribution, Chem. Mater. 24 (2012) 3231–3239, https://doi.org/10.1021/cm301629a.
[88] C.T. Nimlos, A.J. Hoffman, Y.G. Hur, B.J. Lee, J.R. Di Iorio, D.D. Hibbitts, R. Gounder, Experimental and Theoretical Assessments of Aluminum Proximity in MFI Zeolites and Its Alteration by Organic and Inorganic Structure-Directing Agents, Chem. Mater. 32 (2020) 9277–9298, https://doi.org/10.1021/acs.chemmater.0c03154.
[89] Y.G. Hur, P.M. Kester, C.T. Nimlos, Y. Cho, J.T. Miller, R. Gounder, Influence of Tetrapropylammonium and Ethylenediamine Structure-Directing Agents on the Framework Al Distribution in B-Al–MFI Zeolites, Ind. Eng. Chem. Res. 58 (2019) 11849–11860, https://doi.org/10.1021/acs.iecr.9b01726.
[90] R.C. Weast, CRC Handbook of Chemistry and Physics. Sixty-Seventh Edition, CRC Press Inc, Boca Raton, FL (USA), 1986.
[91] A.J. Jones, R.T. Carr, S.I. Zones, E. Iglesia, Acid strength and solvation in catalysis by MFI zeolites and effects of the identity, concentration and location of framework heteroatoms, Journal of Catalysis. 312 (2014) 58–68, https://doi.org/10.1016/j.jcat.2014.01.007.
[92] A. Janda, A.T. Bell, Effects of Si/Al Ratio on the Distribution of Framework Al and on the Rates of Alkane Monomolecular Cracking and Dehydrogenation in H-MFI, J. Am. Chem. Soc. 135 (2013) 19193–19207, https://doi.org/10.1021/ja4081937.
[93] M. Rubeš, E. Koudelková, F.S. de Oliveira Ramos, M. Trachta, O. Bludský, R. Bulánek, Experimental and Theoretical Study of Propene Adsorption on K-FER Zeolites: New Evidence of Bridged Complex Formation, J. Phys. Chem. C. 122 (2018) 6128–6136. https://doi.org/10.1021/acs.jpcc.7b12706.
[94] Y. Shen, Z. Qin, S. Asahina, N. Asano, G. Zhang, S. Qian, Y. Ma, Z. Yan, X. Liu, S. Mintova, The inner heterogeneity of ZSM-5 zeolite crystals, J. Mater. Chem. A. 9 (2021) 4203–4212, https://doi.org/10.1039/D0TA11023J.
[95] W. Qin, Y. Zhou, J.D. Rimer, Deleterious effects of non-framework Al species on the catalytic performance of ZSM-5 crystals synthesized at low temperature, React. Chem. Eng. 4 (2019) 1957–1968, https://doi.org/10.1039/C9RE00231F.
[96] J.C. Groen, T. Bach, U. Ziese, A.M. Paulaime-van Donk, K.P. de Jong, J.A. Moulijn, J. Pérez-Ramírez, Creation of Hollow Zeolite Architectures by Controlled Desilication of Al-Zoned ZSM-5 Crystals, J. Am. Chem. Soc. 127 (2005) 10792–10793, https://doi.org/10.1021/ja052592x.
[97] R. Martínez-Franco, M. Moliner, J.R. Thogersen, A. Corma, Efficient One-Pot Preparation of Cu-SSZ-13 Materials using Cooperative OSDAs for their Catalytic Application in the SCR of NOx, ChemCatChem. 5 (2013) 3316–3323, https://doi.org/10.1002/cctc.201300141.
[98] P. Eliášová, M. Opanasenko, P.S. Wheatley, M. Shamzhy, M. Mazur, P. Nachtigall, W.J. Roth, R.E. Morris, J. Čejka, The ADOR mechanism for the synthesis of new zeolites, Chem. Soc. Rev. 44 (2015) 7177–7206, https://doi.org/10.1039/C5CS00045A.
[99] M. Dusselier, M.E. Davis, Small-Pore Zeolites: Synthesis and Catalysis, Chem. Rev. 118 (2018) 5265–5329, https://doi.org/10.1021/acs.chemrev.7b00738.
[100] M. Kumar, Z.J. Berkson, R.J. Clark, Y. Shen, N.A. Prisco, Z. Zeng, H. Zheng, L.B. McCusker, J.C. Palmer, B.F. Chmelka, J.D. Rimer, Crystallization of Mordenite Platelets using Cooperative Organic Structure-directing Agents jacs.9b09697 J. Am. Chem. Soc. (2019), https://doi.org/10.1021/jacs.9b09697.
[101] T.M. Davis, A.T. Liu, C.M. Lew, D. Xie, A.I. Benin, S. Elomari, S.I. Zones, M.W. Deem, Computationally Guided Synthesis of SSZ-52: A Zeolite for Engine Exhaust Clean-up, Chem. Mater. 28 (2016) 708–711, https://doi.org/10.1021/acs.chemmater.5b04578.
[102] E.M. Gallego, M.T. Portilla, C. Paris, A. León-Escamilla, M. Boronat, M. Moliner, A. Corma, "Ab initio" synthesis of zeolites for preestablished catalytic reactions, Science. 355 (2017) 1051–1054, https://doi.org/10.1126/science.aal0121.
[103] M. Fant, M. Ångqvist, A. Hellman, P. Erhart, To every rule there is an exception: A rational extension of Loewenstein's rule, Angewandte Chemie International Edition. n/a (n.d.). https://doi.org/10.1002/anie.202013256.
[104] R.E. Fletcher, S. Ling, B. Slater, Violations of Löwenstein's rule in zeolites, Chem. Sci. 8 (2017) 7483–7491, https://doi.org/10.1039/C7SC02531A.
[105] C.J. Heard, L. Grajciar, P. Nachtigall, The effect of water on the validity of Löwenstein's rule, Chem. Sci. 10 (2019) 5705–5711, https://doi.org/10.1039/C9SC00725C.
[106] X. Tang, Z. Liu, L. Huang, W. Chen, C. Li, G. Wang, G. Li, X. Yi, A. Zheng, Violation or Abidance of Löwenstein's Rule in Zeolites Under Synthesis Conditions?, ACS Catal. 9 (2019) 10618–10625, https://doi.org/10.1021/acscatal.9b01844.
[107] S.M. Pugh, P.A. Wright, D.J. Law, N. Thompson, S.E. Ashbrook, Facile, Room-Temperature 17O Enrichment of Zeolite Frameworks Revealed by Solid-State NMR Spectroscopy, J. Am. Chem. Soc. 142 (2020) 900–906, https://doi.org/10.1021/jacs.9b10528.
[108] Y. Zhang, Y. Peng, J. Li, K. Groden, J.-S. McEwen, E.D. Walter, Y. Chen, Y. Wang, F. Gao, Probing Active-Site Relocation in Cu/SSZ-13 SCR Catalysts during Hydrothermal Aging by In Situ EPR Spectroscopy, Kinetics Studies, and DFT Calculations, ACS Catal. 10 (2020) 9410–9419, https://doi.org/10.1021/acscatal.0c01590.
[109] J. Luo, F. Gao, K. Kamasamudram, N. Currier, C.H.F. Peden, A. Yezerets, New insights into Cu/SSZ-13 SCR catalyst acidity. Part I: Nature of acidic sites probed by NH3 titration, Journal of Catalysis. 348 (2017) 291–299, https://doi.org/10.1016/j.jcat.2017.02.025.
[110] C.-T. Yang, A. Janda, A.T. Bell, L.-C. Lin, Atomistic Investigations of the Effects of Si/Al Ratio and Al Distribution on the Adsorption Selectivity of *n* -Alkanes in Brønsted-Acid Zeolites, J. Phys. Chem. C. 122 (2018) 9397–9410, https://doi.org/10.1021/acs.jpcc.7b11190.
[111] J.M. Findley, P.I. Ravikovitch, D.S. Sholl, The Effect of Aluminum Short-Range Ordering on Carbon Dioxide Adsorption in Zeolites, J. Phys. Chem. C. 122 (2018) 12332–12340, https://doi.org/10.1021/acs.jpcc.8b03475.